

Article

# Characterization of Titanium Surface Modification Strategies for Osseointegration Enhancement

Jinyoung Kim <sup>1,†</sup>, Hyun Lee <sup>2,3,†</sup>, Tae-Sik Jang <sup>4</sup>, DongEung Kim <sup>5</sup>, Chang-Bun Yoon <sup>6</sup>, Ginam Han <sup>2,3</sup> ,  
Hyoun-Ee Kim <sup>1</sup> and Hyun-Do Jung <sup>2,3,\*</sup> 

<sup>1</sup> Department of Materials Science and Engineering, Seoul National University, Seoul 08826, Korea; tmr002@snu.ac.kr (J.K.); kimhe@snu.ac.kr (H.-E.K.)

<sup>2</sup> Department of BioMedical-Chemical Engineering (BMCE), The Catholic University of Korea, Bucheon 14662, Korea; leeh0520@catholic.ac.kr (H.L.); gnhan@catholic.ac.kr (G.H.)

<sup>3</sup> Department of Biotechnology, The Catholic University of Korea, Bucheon 14662, Korea

<sup>4</sup> Department of Materials Science and Engineering, Chosun University, Gwangju 61452, Korea; tsjang@chosun.ac.kr

<sup>5</sup> Research Institute of Advanced Manufacturing Technology, Korea Institute of Industrial Technology, Incheon 21999, Korea; canon@kitech.re.kr

<sup>6</sup> Department of Advanced Materials Engineering, Korea Polytechnic University, Siheung 15073, Korea; cbyoon@kpu.ac.kr

\* Correspondence: hdjung@catholic.ac.kr; Tel.: +82-2-2164-4357

† Jinyoung Kim and Hyun Lee have contributed equally to this work.

**Abstract:** As biocompatible metallic materials, titanium and its alloys have been widely used in the orthopedic field due to their superior strength, low density, and ease of processing. However, further improvement in biological response is still required for rapid osseointegration. Here, various Ti surface-treatment technologies were applied: hydroxyapatite blasting, sand blasting and acid etching, anodic oxidation, and micro-arc oxidation. The surface characteristics of specimens subjected to these techniques were analyzed in terms of structure, elemental composition, and wettability. The adhesion strength of the coating layer was also assessed for the coated specimens. Biocompatibility was compared via tests of in vitro attachment and proliferation of pre-osteoblast cells.

**Keywords:** titanium; surface treatment; HA blasting; sandblasted and acid-etched (SLA); anodic oxidation (AO); micro-arc oxidation (MAO)



**Citation:** Kim, J.; Lee, H.; Jang, T.-S.; Kim, D.; Yoon, C.-B.; Han, G.; Kim, H.-E.; Jung, H.-D. Characterization of Titanium Surface Modification Strategies for Osseointegration Enhancement. *Metals* **2021**, *11*, 618. <https://doi.org/10.3390/met11040618>

Academic Editor: Francesca Borgioli

Received: 6 March 2021

Accepted: 8 April 2021

Published: 11 April 2021

**Publisher's Note:** MDPI stays neutral with regard to jurisdictional claims in published maps and institutional affiliations.



**Copyright:** © 2021 by the authors. Licensee MDPI, Basel, Switzerland. This article is an open access article distributed under the terms and conditions of the Creative Commons Attribution (CC BY) license (<https://creativecommons.org/licenses/by/4.0/>).

## 1. Introduction

Various materials have been used as biomaterials to replace damaged organs or tissues inside the human body. Different materials have been chosen for application to different damaged body parts based on the intrinsic properties of each material. Such materials are classified into three main groups: metals, ceramics, and polymers. Metals and ceramics have been applied mostly to hard tissue engineering, because its inherent mechanical properties are sufficient to endure applied loads [1,2]. By contrast, polymers have been broadly utilized in soft and hard tissue engineering, since their properties are determined by not only molecular weight and fabrication method but also constituent elements and chain structure [3,4]. Among these, metallic materials have been more widely used as hard tissue substitutes than ceramics or polymers because of their excellent mechanical properties, chemical stability in physiological conditions, and ductility, which can prevent sudden fracture [5,6]. Given biocompatibility considerations, the most prevalently facilitated metallic materials have been stainless steel (SUS) [7], Co–Cr alloys [8], magnesium (Mg) [9], and titanium and its alloys [10–13].

Titanium and its alloys are the most extensively utilized metals because of their excellent biocompatibility, high strength-to-weight ratios, and ease of processing, in addition to

the characteristics of metals mentioned earlier [5,14,15]. Unlike other biologically compatible metals, Ti and Ti alloys exhibit exceptional corrosion resistance due to the formation of a passive oxide film layer [16]. This TiO<sub>2</sub> layer, bonded tightly to Ti, greatly increases resistance to all types of corrosion while simultaneously improving cellular compatibility [5,14]. Furthermore, Ti alloys including Ti–6Al–4V [17,18], Ti–Nb–Zr [19,20], and Ti–Nb–Zr–Ta alloys [21,22] have been developed for increased strength, enhanced biocompatibility, and reduced elastic modulus, respectively, using theoretical calculations to consider the effect of each element (DV-X $\alpha$ ) [23,24]. The effectiveness of each of these Ti alloys has already been studied and demonstrated [25–28].

Even though Ti and Ti alloys exhibit suitable properties for utilization as biomaterials, there remains a potential improvement in biocompatibility for long-term stability. Fast-paced research aimed at solving these problems through surface treatment of Ti and Ti alloys is already under way [29–32]. One commonly implemented method is to increase osseointegration by surface coating with various materials such as calcium phosphate for improved biocompatibility. In another method, micro- or nano-level roughness is added to the surface structure, and an oxide layer is intentionally created to maximize the effect. Increasing the surface roughness improves cell characteristics [33,34] and the stability of the implant [35], and it can be used for drug loading or as an antibacterial coating layer [36–38]. The formation of a calcium phosphate-based coating layer on titanium for various purposes has been widely studied [5,39]. It is known that the sand blasting and acid etching (SLA) method, which is the most often used strategy to alter the surface structure of titanium, not only increases biometric characteristics by increasing the roughness [40] but also is suitable for implants requiring mechanical strength [41]. In some studies, however, SLA specimens exhibited poorer cellular properties than those of specimens with a smooth surface [42]. Furthermore, granules and etching agents that were not completely removed after SLA treatment could affect the osteointegration of the implant [43]. Therefore, in addition to SLA, a method such as target ion-induced plasma sputtering can be used to increase the biocompatibility by increasing the roughness [44], and the structure of the surface layer can thus be made more suitable for implants through anodic oxidation (AO) and micro arc oxidation (MAO) methods that use electrical treatment to intentionally create an oxide layer [45,46].

In this study, HA blasting and SLA was firstly applied to prepare surface-treated Ti substrates (noted as HA and SLA). Then AO and MAO processes were additionally conducted on the SLA-treated Ti specimens to form a supplementary titanium dioxide layer (noted as SLA/AO and SLA/MAO). The physiological and biological properties were compared through the following methods. The microstructure of the surface and the coating thickness were assessed through field-emission scanning electron microscopy (FE-SEM) with a focused ion beam (FIB). Elemental alteration was confirmed through X-ray diffraction (XRD) and energy-dispersive X-ray spectroscopy (EDS). Furthermore, the roughness of the surface-treated Ti specimens was evaluated by laser scanning microscopy (LSM), and the hydrophilicity of specimens was also measured. Coating layers were formed using a sequence of hydroxyapatite (HA) blasting, AO, and MAO, and the stability of each layer was estimated. In vitro tests of attachment and proliferation were conducted to compare the effectiveness of various surface-treatment techniques.

## 2. Materials and Methods

### 2.1. Preparation of Surface-Treated Ti Substrates

Commercially available Ti plates (Commercially pure Ti G4) were prepared with dimensions of 10 mm  $\times$  10 mm  $\times$  2 mm. Ti plates were sequentially polished using P400, P1000, and P2000 SiC papers. After polishing, Ti plates were washed in ethanol under sonication to remove debris and then dried at a temperature below 70 °C prior to surface treatment. In the preparation of HA-blasted Ti plates (hereafter HA), Ti plates were impacted by jetted HA particles and then rinsed with nitric acid to eliminate remaining HA sandblasting particles. In the case of SLA treatment, an identical HA-blasting procedure

was conducted prior to the following post-treatment. Nitric acid-treated Ti plates were immersed in a 5 M NaOH solution for 24 h at 60 °C and then soaked in distilled water for 24 h at 80 °C. Specimens were then dried in an oven overnight at 40 °C, followed by heat treatment at 600 °C for 1 h of dwelling time. AO and MAO procedures were applied to form a titanium oxide (TiO<sub>2</sub>) layer on the SLA-Ti surface. The MAO process used an electrolytic solution containing 0.25 wt% ammonium fluoride (Sigma-Aldrich, Saint Louis, MO, USA), whereas the AO process used a solution of 98 vol% ethylene glycol (Sigma-Aldrich) and 2 vol% distilled water. SLA-treated Ti plates were dipped in the prepared electrolytic solution, and a DC field (HD-9001D, FinePower, Seoul, Korea) of 60 V was applied for 30 min. Fabricated SLA/AO-Ti plates were ultrasonically cleaned sequentially in acetone, ethanol, and distilled water. MAO treatment was performed in an electrolytic aqueous solution of 0.15 M calcium acetate monohydrate (Sigma-Aldrich) and 0.02 M glycerol phosphate calcium salt (Sigma-Aldrich). Electric power from a pulsed DC field (Pulse Power Supply; Model-P6241, Auto Electric Co., Seoul, Korea) was supplied to the specimens and the stainless steel (SUS) counter electrode for 2 min under the following conditions: voltage, 350 V; frequency, 660 Hz; and 60% duty. A cooling bath at 10 °C was utilized to prevent temperature rise during the process. After treatment, SLA/MAO-Ti plates were again rinsed with distilled water and ethanol.

## 2.2. Characterization of Ti Substrates after Surface Treatments

The surface morphologies of prepared surface-treated Ti plates were analyzed using FE-SEM (JSM-6330F, JEOL, Tokyo, Japan). For each of HAs, SLA/AO, and SLA/MAO, the structure and thickness of the coating layer were observed using a FIB (AURIGA, Carl Zeiss, Oberkochen, Germany) to section the coating layer. An elemental analysis was conducted by EDS equipped with FE-SEM, and the crystalline phases of each specimen were analyzed using XRD (D8-advance, BRUKER Co., Billerica, MA, USA) with 20–80° of scanning range and a 1°/min scanning rate. Additionally, the hydrophilicity of surface-treated Ti plates was assessed by measuring the aqueous wetting angle using a contact angle analyzer (Phoenix 300; Surface Electro Optics Co., Suwon, Korea). In total, 10 µL of distilled water droplets were dropped onto each surface from a syringe, and the morphology of the water droplet was monitored at particular time intervals: 0 min, 2 min, 6 min, and 10 min. The wetting angle was estimated by using an image analysis program (Image XP). The surface roughness of prepared surface-treated Ti plates was analyzed by LSM (OLS 3100, Olympus, Tokyo, Japan). The surface root mean square height (Sq) was determined for a surface area of 1280 × 1280 µm<sup>2</sup> using a 5× objective lens at a wavelength of 408 nm. The adhesive strength between the coating layer and the Ti substrate was measured using the pull-out test, and three specimens for each condition were examined. Aluminum studs with pre-epoxy coating were attached to each surface and heated at 150 °C to cure the epoxy. Studs attached to each coating were pulled until detachment by a universal testing machine (RB302 single column type; R&B, Daejeon, Korea) at a rate of 1 mm/min. The remaining coating layers were observed by FE-SEM after detachment.

## 2.3. In Vitro Biocompatibility Assessment

In vitro cell tests, including attachment and proliferation tests, were carried out to assess the biocompatibility of treated Ti substrates. Sequential sterilization by immersion in 70%EtOH, autoclaving at 121 °C, and UV irradiation were performed on all of the specimens before the tests. Pre-osteoblast cells (MC3T3-E1; ATCC, CRL-2593, Manassas, VA, USA) were cultured in the alpha-minimum essential medium (α-MEM; Welgene Co., Gyeongsan, Korea) containing 10% fetal bovine serum (FBS; Gibco, New York, NY, USA) and 1% penicillin–streptomycin (Pen–strep; Gibco) in a humidified incubator at 37 °C and a CO<sub>2</sub> concentration below 5%. For cell attachment assessment, prepared specimens were immersed in a medium containing 3 × 10<sup>4</sup> cells per mL. After 3 h of culturing, adhered cells were fixed by 2.5% glutaraldehyde (Sigma-Aldrich) and dehydrated using 75%, 95%, and 100% EtOH, as well as 1,1,1,3,3,3-hexamethyldisilazane (Sigma-Aldrich). The morphology

of cells was observed by FE-SEM. The degree of cell proliferation was measured after the methoxyphenyl tetrazolium salt (MTS) method was carried out. A total of  $3 \times 10^4$  cells/mL were cultured on the treated Ti substrates for 3 days and 5 days. Three specimens of each group were tested. For each incubation time, specimens were rinsed twice with DPBS (Dulbecco's phosphate buffered saline; Welgene Co.) to remove non-attached cells. The specimens were then immersed in FBS-free  $\alpha$ -MEM containing a 10% cell proliferation assay kit solution (CellTiter 96 Aqueous One Solution Cell Proliferation Assay) and cultivated in an incubator to induce sufficient reaction. Afterward, the absorbance of the medium was measured using a microplate reader (EX read 400, Biochrom, Hollistone, MA, UK) at a wavelength of 490 nm.

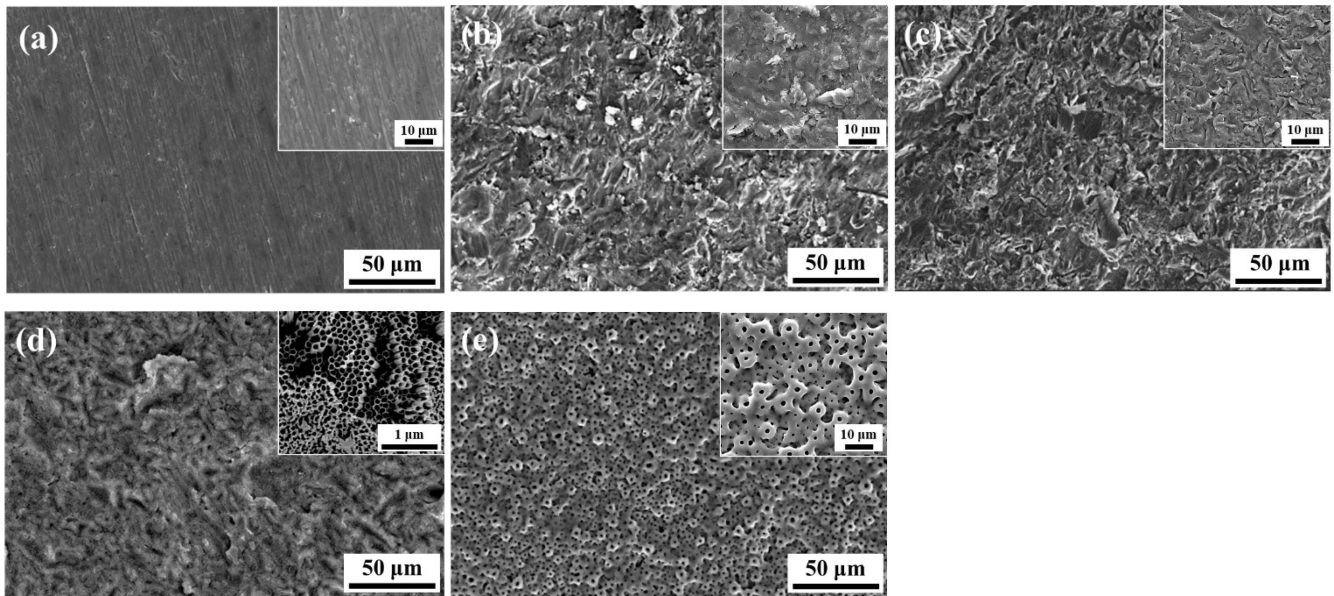
#### 2.4. Statistical Analysis

Statistical analysis was carried out using statistical package for the social sciences (SPSS 27, SPSS Inc., Chicago, IL, USA). One-way analysis of variance with Tukey post hoc was performed to the results of adhesion strength, and Kruskal-Wallis H test with pairwise comparison post hoc was conducted on the cell proliferation data. The  $p$  values less than 0.05 were considered statistically significant.

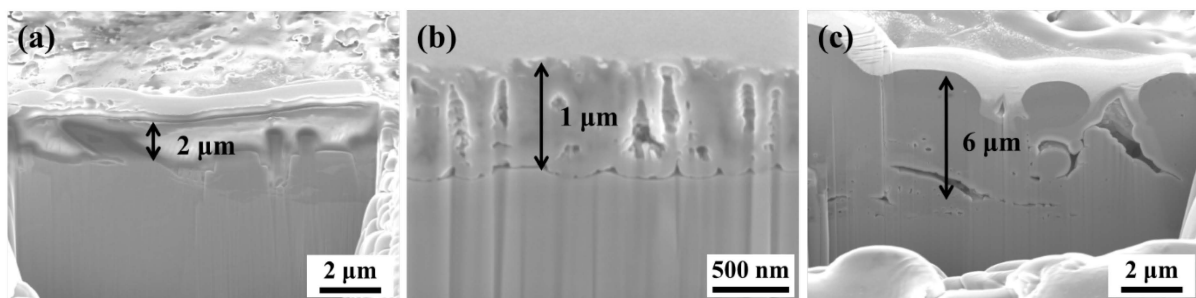
### 3. Results and Discussion

Figure 1 illustrates FE-SEM observations of the surface structures of surface-treated Ti specimens. The unique polishing pattern is clearly visible in the Ti specimen (Figure 1a). By contrast, the HA-blasted specimens and SLAs in Figure 1b,c show surfaces roughened by the blasting and acid treatment process. The highly magnified image indicates a sharply carved surface morphology derived from blasting and etching. Contrarily, unique structures were observed in the two experimental groups that underwent additional surface treatment through electro-oxidation. As demonstrated in Figure 1d, considerable differences were not found between SLA/AO specimens and HA and SLA specimens based on low-magnification images. However, as indicated in the inset image, nanoporous rods were generated on the SLA-treated Ti surface; this phenomenon is typical in AO treatment [34,44]. Meanwhile, trace of SLA treatment could not be seen in the SLA/MAO specimens (Figure 1e), and a typical crater-like porous structure was formed on the surface. This structure was generated by the numerous arcs on the Ti surface during the MAO treatment process, and the structure and its shapes are consistent with structures documented in various MAO studies [47,48]. This finding suggests that the additional treatment to SLA-treated Ti substrates could induce a more roughened structure or formation of a coating layer.

Unlike the SLA-treated specimens, which removed foreign substances from the surface through an acid treatment process, the HA samples and the samples treated with AO and MAO after SLA exhibited coating layers with different thicknesses. Coating layer thicknesses for HA-, SLA/AO-, and SLA/MAO-treated Ti surfaces were identified through FIB (Figure 2). Since surface treatments were performed in optimized conditions with effectiveness, the thicknesses of the formed coating layers differed. The average measured thickness for each group was 6  $\mu\text{m}$ , 2  $\mu\text{m}$ , and 1  $\mu\text{m}$  for SLA/MAO, HA, and SLA/AO, respectively. According to Wu and Kuromoto, the thickness of the coating layer of AO changes according to the anodizing time and volume [49,50]; conditions applied here yielded a thickness of approximately 1  $\mu\text{m}$ . MAO-treated specimens exhibited a thicker coating layer than AO-treated ones because the applied bias voltage was much higher in MAO treatment (350 V) than that in AO treatment (60 V). This difference resulted in a far more intense electric reaction on the Ti surface in the electrolyte for MAO than that for AO.



**Figure 1.** Surface morphology of surface-modified Ti through various treatments: (a) Ti, (b) hydroxyapatite blasting (HA), (c) sandblasted and acid-etched (SLA), (d) SLA/anodic oxidation (AO), and (e) SLA/micro arc oxidation (MAO).



**Figure 2.** Focused ion beam (FIB) images of surface-modified Ti: (a) HA, (b) SLA/AO, and (c) SLA/MAO.

The elemental characteristics of each experimental condition were analyzed through XRD and EDS analyses. Figure 3a illustrates the crystalline phases of each Ti substrate after surface treatment. Compared to the crystalline phases of pristine Ti, SLA-treated Ti specimens exhibited identical results, since all of the undesired residues were eliminated after SLA treatment [40]. By contrast, HA-Ti specimens exhibited representative HA peaks because HA particles were embedded into the Ti substrate. Specimens treated by electrical discharge exhibited peaks related to anatase  $\text{TiO}_2$ . However, in SLA/AO, the  $\text{TiO}_2$  peak was not clearly observed because the  $\text{TiO}_2$  formed through anodizing was in an amorphous state [34]. Furthermore, Figure 3b exhibits embedded elements on the specimen surfaces, and only HA- and SLA/MAO-treated Ti surfaces exhibited evidence of the Ca and P elements. These Ca and P peaks emerged because oxidation by the generated electric arc caused HA particles (HA treated Ti) to be embedded, incorporating Ca and P in the  $\text{TiO}_2$  coating layer (SLA/MAO-treated Ti) [51,52].

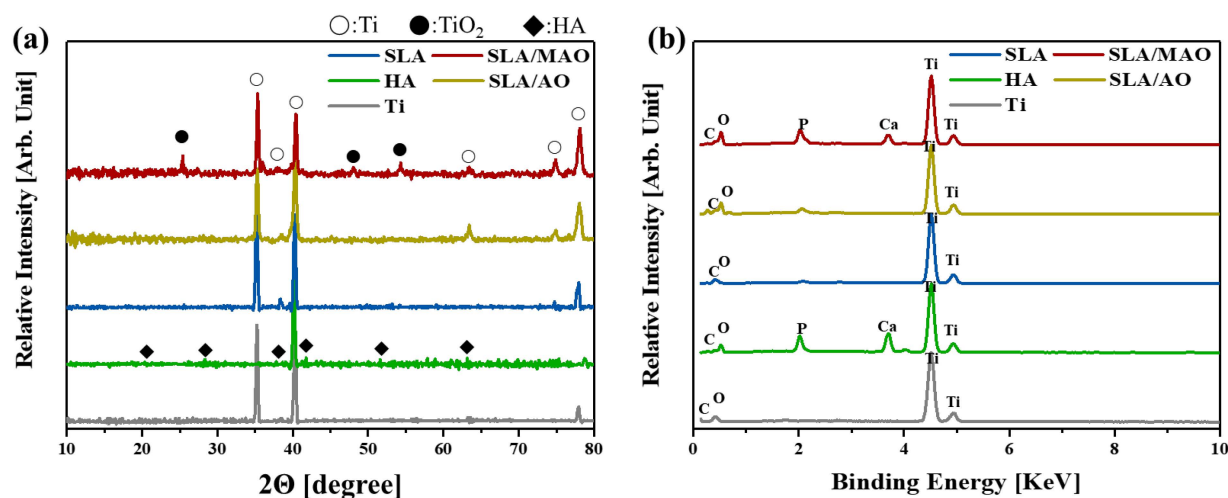


**Figure 3.** Component analysis of surface-modified titanium through (a) X-ray diffraction (XRD) and (b) energy-dispersive X-ray spectroscopy (EDS) analyses.

For good osseointegration between the artificial implant and the surrounding bones, a roughened surface is required, since the initial adhesion of osteoblasts is thereby improved; surrounding irregularities promote the differentiation of stem cells into bone cells [53]. Since the experimental methods for treating Ti surfaces in this study have been acknowledged as useful ways of creating rough surfaces, a quantitative roughness assessment was conducted. Figure 4 presents LSM images of treated surfaces; Table 1 summarizes the LSM-measured  $S_q$  values. As illustrated in Figure 4, the pristine Ti exhibited an almost flat state. The SLA specimen exhibited minimal roughness. All of the experimental groups displayed a significantly higher degree of roughness than pristine Ti. HA specimens (Figure 4b) were much rougher because of the carving and fixation of HA particles resulting from collisions between HA particles and the Ti surface. SLA-treated specimens showed higher  $S_q$  value than pure Ti as illustrated in Figure 4c with evenly distributed color map. The SLA/AO specimens indicated slightly higher roughness than SLA group because of the generated topmost nanoporous TiO<sub>2</sub> layer. The most roughened surfaces were specimens treated using SLA/MAO, as is clear from the drastic color distribution in Figure 4e. A highly drastic reaction occurring on the Ti surface induced an irregularly distributed TiO<sub>2</sub> coating layer with crater-like micropores.

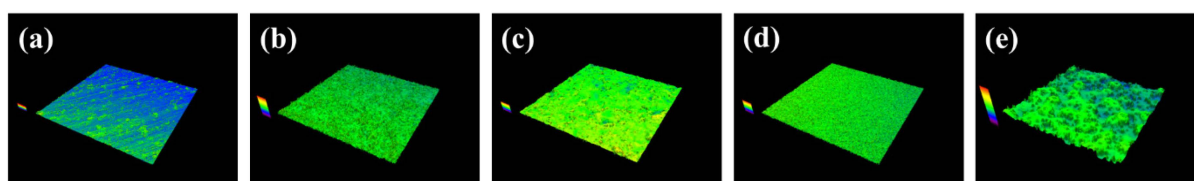


**Figure 4.** Roughness of surface-modified Ti: (a) Ti, (b) HA, (c) SLA, (d) SLA/AO, and (e) SLA/MAO.

**Table 1.**  $S_q$  value of surface-modified Ti.

Specimens	Ti	HA	SLA	SLA/AO	SLA/MAO
$S_q$ ( $\mu\text{m}$ )	$0.198 \pm 0.032$	$0.729 \pm 0.070$	$0.544 \pm 0.106$	$0.632 \pm 0.056$	$0.825 \pm 0.148$

Surface hydrophilicity, which is one of the key factors promoting cellular response, was confirmed by monitoring the contact angle (Figure 5). The contact angle was assessed at particular intervals because wettability is a time-dependent feature after initial wetting of the surface [54]. The contact angle, which represents the degree of hydrophilicity, tends to decrease as the roughness increased for surface-treated Ti specimens. Among the vari-

ous specimens, the HA specimen exhibited a similar level of hydrophilicity to that of the SLA/MAO specimen because HA present on the surface is known to produce good hydrophilicity. Significant hydrophilicity difference was not observed in SLA/AO compared to Ti. Nonetheless, SLA/AO specimens, whose roughness was greater than that of SLA specimens, showed greater hydrophilicity than that of SLA specimens. Previous research demonstrated that the application of SLA reduces the wettability of Ti [55], whereas the application of MAO increases the wettability of Ti [54]. This tendency was clearly confirmed by Figure 5b, which indicates that hydrophilicity was considerably greater for HA and SLA/MAO specimens than for other specimens in every case. This finding suggests that HA and SLA/MAO specimens would display the most desirable cellular behavior. In particular, contact angles on HA and SLA/MAO specimens decreased with time due to the ease of penetration of the micro-sized irregularities [54]. Various studies reported that an increase in wettability enhances cellular properties [56,57].

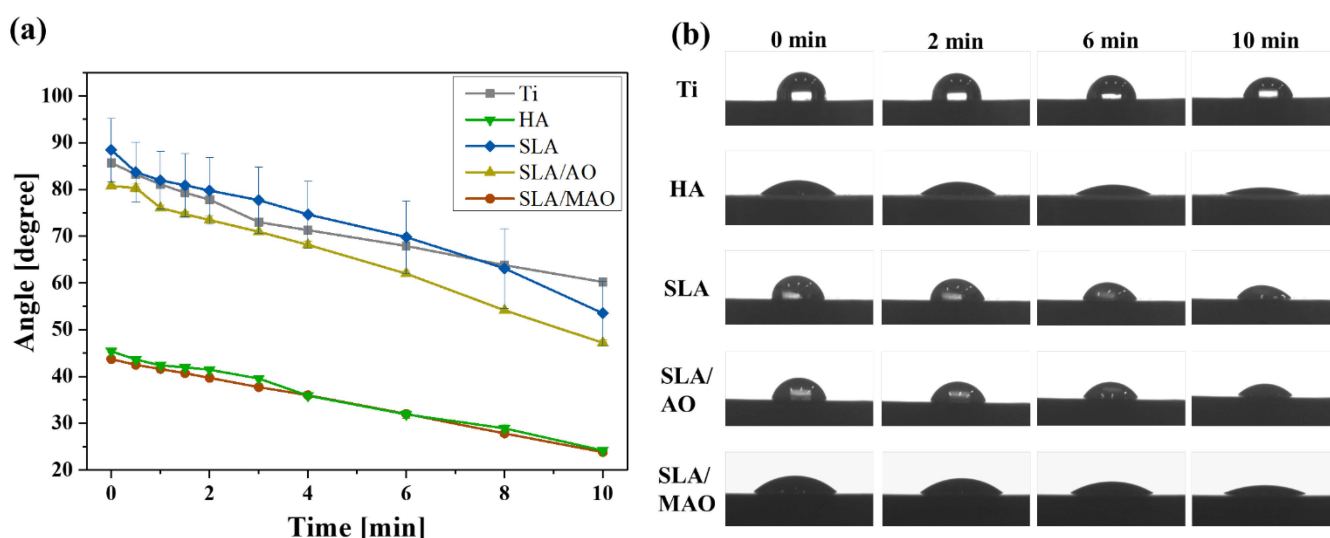


**Figure 5.** Measurement of wettability of surface-modified Ti through contact angle with water: (a) graph of the change in contact angle of each specimen over time and (b) monitored morphology of water drops on each specimen following dwelling time.

As a method to compare the stability of the coating, adhesion strength was measured using a pull-out test, which is suitable for measuring the required force for the removal of the coating from the substrate [58–60]. As suggested in Figure 6a–c, the coating layer could be clearly distinguished from the detached parts following the contours (red dashed line). Compared to HA and SLA/AO specimens, SLA/MAO specimens showed a more rugged boundary morphology along the remaining coating layer because of the much thicker  $\text{TiO}_2$  layer due to MAO, as illustrated in Figure 2. Measured adhesion strengths were noted in Figure 6d: Adhesion in electrically treated specimens (SLA/AO and SLA/MAO) was significantly tighter than that in HA specimens. Unlike AO and MAO, HA is based mainly on physical treatment that induces collisions between accelerated HA particles and the target substrate. This difference led to a weaker bonding strength for HA than that for SLA/AO or SLA/MAO. The adhesion strength of the HA layer to the Ti substrate was comparable to that of a Polyetherimide (PEI) coating on Ti, since both of coating layers were physically entangled with the Ti substrate.

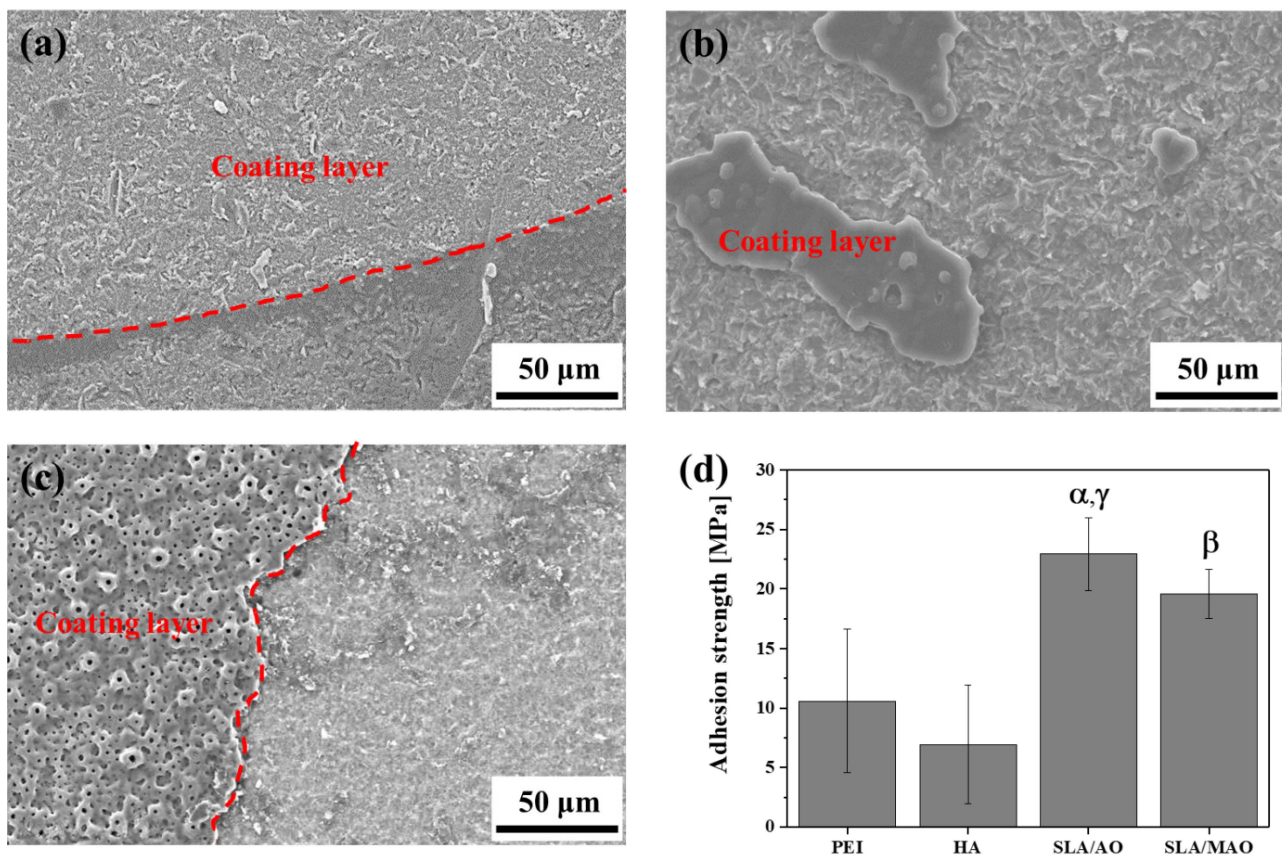


**Figure 6.** Surface morphology after detachment of coating layer of (a) HA, (b) SLA/AO, and (c) SLA/MAO. (d) quantitatively measured adhesion strength ( $\alpha$  denotes  $p < 0.05$  compared to PEI,  $\beta$  denotes  $p < 0.05$  and  $\gamma$  denotes  $p < 0.01$  compared to HA).

Results of in vitro tests of biocompatibility are illustrated in Figure 7. SEM images of the adhered cells after 3 h of incubation are presented in Figure 7a–e. The attached cells exhibited well-spread shapes on all of the specimens, demonstrating that the selected techniques were not cytotoxic to the cells. Since Ti itself is one of the metals with good cell affinity, an excellent degree of cell adhesion was found. Among the surface-treated specimens, the cells were found to be spreading more filopodia toward the surfaces in HA and SLA/MAO specimens, which showed high extent of surface roughness. In the case of the HA specimen, both the chemical similarity to the bone and the physically roughened surface complexly affected cellular behavior. When SLA, SLA/AO, and SLA/MAO were compared, the extension of cells was high in SLA/AO and SLA/MAO, driven by the increased roughness of the additional TiO<sub>2</sub> layer. Cell characteristics are generally known to be affected by the roughness and topography of the surface structure [29,61]. According to several previous studies regarding surface treatment on Ti, cell affinity is improved when surface area and surface roughness are enhanced by a nanotube structure or micron-sized roughness such as SLA/AO or SLA/MAO [62,63]. By contrast, the inter-treatment pattern in degree of proliferation was different from the pattern in cell attachment. Figure 7f illustrates cell viability as assessed by the MTS assay after 3 days or 5 days of culturing on each specimen. Measured cell viability at 3 days of culturing time presented a similar degree of cell proliferation, indicating that adhered cells multiplied comparably in the early stage. However, the obtained cell viability at 5 days of culturing had a different trend. Except for HA, cells proliferated considerably in all of the experimental groups; surface-treated Ti specimens provided an environment for cell growth preferable to that of pristine Ti specimens. In HA-Ti specimens, the instability of the coating layer, as inferred from the lower adhesion strength, may have resulted in an insecure state, slowing the

proliferation of cells. According to Brodie et al., even if the same coating layer exists on the surface, the poor stability of the coating layer adversely affects cell proliferation [64]. The other specimens, whose coating layers were stable, differed meaningfully only in surface structure and composition, and all had a greater degree of proliferation than pristine Ti.

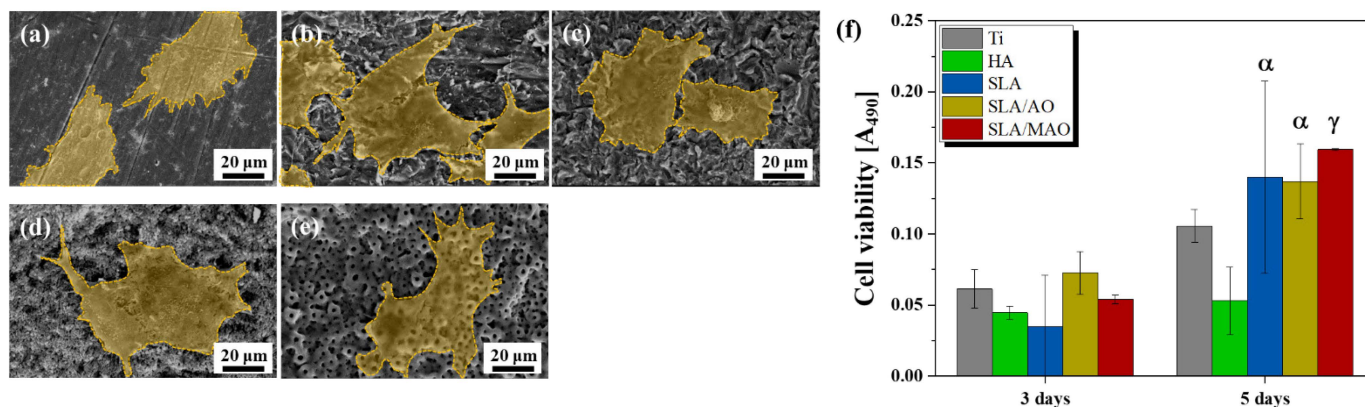


**Figure 7.** SEM images of attached pre-osteoblast cells on (a) Ti, (b) HA, (c) SLA, (d) SLA/AO, (e) SLA/MAO, and (f) measured degree of cell proliferation ( $\alpha$  denotes  $p < 0.05$  and  $\gamma$  denotes  $p < 0.01$  compared to HA at 5 days).

#### 4. Conclusions

In this study, four of the most prevalent surface treating strategies for Ti were systematically compared: HA-blasting, SLA, SLA/AO, and SLA/MAO. After surface treatment, each of the specimens exhibited a substantially roughened surface structure due to the additional coating layer or carving process. Elemental components were analyzed by EDS and XRD, confirming that Ti, HA, and TiO<sub>2</sub> layers were present, in agreement with previous research. Surface-treated Ti substrates exhibited higher hydrophilicity than that of pristine Ti substrates as a result of increased roughness and porosity. Furthermore, adhesion strength tests indicated that the HA coating layer was less stable than the TiO<sub>2</sub> layer formed through AO and MAO. In vitro test results demonstrated the superiority of electrical treatments (SLA/AO and SLA/MAO) in enhancing cellular attachment and proliferation.

**Author Contributions:** Conceptualization, T.-S.J. and H.-D.J.; methodology, H.L., D.K., C.-B.Y., G.H.; validation, J.K., H.-D.J.; investigation, J.K., H.L., C.-B.Y., G.H.; resources, H.L., D.K., H.-D.J.; data curation, J.K., H.L., H.-D.J.; writing—original draft preparation, J.K., H.L.; writing—review and editing, J.K., H.L., H.-D.J.; supervision, H.-E.K., H.-D.J.; project administration, H.-D.J.; funding acquisition, H.-E.K., H.-D.J.; All authors have read and agreed to the published version of the manuscript.

**Funding:** This work was supported by The Catholic University of Korea, Research Fund, 2020 and the Basic Science Research Program [No. 2020R1F1A1072103] through the National Research Foundation of Korea funded by the Korea government (MSIT).

**Institutional Review Board Statement:** Not applicable.

**Informed Consent Statement:** Not applicable.

**Data Availability Statement:** Not included.

**Conflicts of Interest:** The authors declare no conflict of interest.

#### References

1. Paital, S.R.; Dahotre, N.B. Calcium phosphate coatings for bio-implant applications: Materials, performance factors, and methodologies. *Mater. Sci. Eng. R Rep.* **2009**, *66*, 1–70. [[CrossRef](#)]
2. An, S.-H.; Matsumoto, T.; Miyajima, H.; Nakahira, A.; Kim, K.-H.; Imazato, S. Porous zirconia/hydroxyapatite scaffolds for bone reconstruction. *Dent. Mater.* **2012**, *28*, 1221–1231. [[CrossRef](#)]

3. Park, S.-B.; Lih, E.; Park, K.-S.; Joung, Y.K.; Han, D.K. Biopolymer-based functional composites for medical applications. *Prog. Polym. Sci.* **2017**, *68*, 77–105. [[CrossRef](#)]
4. Tan, A.C.W.; Polo-Cambrenell, B.J.; Provaggi, E.; Ardila-Suárez, C.; Ramirez-Caballero, G.E.; Baldovino-Medrano, V.G.; Kalaskar, D.M. Design and development of low cost polyurethane biopolymer based on castor oil and glycerol for biomedical applications. *Biopolymers* **2017**, *109*, e23078. [[CrossRef](#)]
5. Jaafar, A.; Hecker, C.; Árki, P.; Joseph, Y. Sol-Gel Derived Hydroxyapatite Coatings for Titanium Implants: A Review. *Bioengineering* **2020**, *7*, 127. [[CrossRef](#)]
6. Hashemi, R. Failure Analysis of Biometals. *Metals* **2020**, *10*, 662. [[CrossRef](#)]
7. Kato, K.; Yamamoto, A.; Ochiai, S.; Wada, M.; Daigo, Y.; Kita, K.; Omori, K. Cytocompatibility and mechanical properties of novel porous 316L stainless steel. *Mater. Sci. Eng. C* **2013**, *33*, 2736–2743. [[CrossRef](#)]
8. Shah, F.A.; Omar, O.; Suska, F.; Snis, A.; Matic, A.; Emanuelsson, L.; Norlindh, B.; Lausmaa, J.; Thomsen, P.; Palmquist, A. Long-term osseointegration of 3D printed CoCr constructs with an interconnected open-pore architecture prepared by electron beam melting. *Acta Biomater.* **2016**, *36*, 296–309. [[CrossRef](#)]
9. Li, N.; Zheng, Y. Novel Magnesium Alloys Developed for Biomedical Application: A Review. *J. Mater. Sci. Technol.* **2013**, *29*, 489–502. [[CrossRef](#)]
10. Takemoto, M.; Fujibayashi, S.; Neo, M.; Suzuki, J.; Kokubo, T.; Nakamura, T. Mechanical properties and osteoconductivity of porous bioactive titanium. *Biomaterials* **2005**, *26*, 6014–6023. [[CrossRef](#)]
11. Carlsson, L.; Röstlund, T.; Albrektsson, B.; Albrektsson, T.; Brånemark, P.-I. Osseointegration of titanium implants. *Acta Orthop. Scand.* **1986**, *57*, 285–289. [[CrossRef](#)]
12. Shah, F.A.; Trobos, M.; Thomsen, P.; Palmquist, A. Commercially pure titanium (cp-Ti) versus titanium alloy (Ti6Al4V) materials as bone anchored implants—Is one truly better than the other? *Mater. Sci. Eng. C* **2016**, *62*, 960–966. [[CrossRef](#)]
13. Prachar, P.; Bartáková, S.; Vanek, J. The titanium PV I endosteal implant from beta-titanium alloy Ti 38Nb 6Ta. *Biomed. Pap.* **2015**, *159*, 503–507. [[CrossRef](#)]
14. Niinomi, M.; Nakai, M.; Hieda, J. Development of new metallic alloys for biomedical applications. *Acta Biomater.* **2012**, *8*, 3888–3903. [[CrossRef](#)]
15. Wally, Z.J.; Van Grunsven, W.; Claeysens, F.; Goodall, R.; Reilly, G.C. Porous Titanium for Dental Implant Applications. *Metals* **2015**, *5*, 1902–1920. [[CrossRef](#)]
16. Aziz-Kerrzo, M.; Conroy, K.G.; Fenelon, A.M.; Farrell, S.T.; Breslin, C.B. Electrochemical studies on the stability and corrosion resistance of titanium-based implant materials. *Biofabrication* **2001**, *22*, 1531–1539. [[CrossRef](#)]
17. Cheng, A.; Humayun, A.; Cohen, D.J.; Boyan, B.D.; Schwartz, Z. Additively manufactured 3D porous Ti-6Al-4V constructs mimic trabecular bone structure and regulate osteoblast proliferation, differentiation and local factor production in a porosity and surface roughness dependent manner. *Biofabrication* **2014**, *6*, 045007. [[CrossRef](#)]
18. Nune, K.C.; Kumar, A.; Misra, R.D.K.; Li, S.J.; Hao, Y.L.; Yang, R. Osteoblast functions in functionally graded Ti-6Al-4 V mesh structures. *J. Biomater. Appl.* **2015**, *30*, 1182–1204. [[CrossRef](#)]
19. He, Y.; Zhang, Y.; Meng, Z.; Jiang, Y.; Zhou, R. Microstructure evolution, mechanical properties and enhanced bioactivity of Ti-Nb-Zr based biocomposite by bioactive calcium pyrophosphate. *J. Alloy. Compd.* **2017**, *720*, 567–581. [[CrossRef](#)]
20. Ozan, S.; Lin, J.; Li, Y.; Ipek, R.; Wen, C. Development of Ti-Nb-Zr alloys with high elastic admissible strain for temporary orthopedic devices. *Acta Biomater.* **2015**, *20*, 176–187. [[CrossRef](#)]
21. Cordeiro, J.M.; Nagay, B.E.; Ribeiro, A.L.R.; da Cruz, N.C.; Rangel, E.C.; Fais, L.M.; Vaz, L.G.; Barão, V.A. Functionalization of an experimental Ti-Nb-Zr-Ta alloy with a biomimetic coating produced by plasma electrolytic oxidation. *J. Alloy. Compd.* **2019**, *770*, 1038–1048. [[CrossRef](#)]
22. Stráský, J.; Harcuba, P.; Václavová, K.; Horváth, K.; Landa, M.; Srba, O.; Janeček, M. Increasing strength of a biomedical Ti-Nb-Ta-Zr alloy by alloying with Fe, Si and O. *J. Mech. Behav. Biomed. Mater.* **2017**, *71*, 329–336. [[CrossRef](#)] [[PubMed](#)]
23. Kolli, R.P.; Devaraj, A. A Review of Metastable Beta Titanium Alloys. *Metals* **2018**, *8*, 506. [[CrossRef](#)]
24. Chen, L.-Y.; Cui, Y.-W.; Zhang, L.-C. Recent Development in Beta Titanium Alloys for Biomedical Applications. *Metals* **2020**, *10*, 1139. [[CrossRef](#)]
25. Lee, H.; Jung, H.-D.; Kang, M.-H.; Song, J.; Kim, H.-E.; Jang, T.-S. Effect of HF/HNO<sub>3</sub>-treatment on the porous structure and cell penetrability of titanium (Ti) scaffold. *Mater. Des.* **2018**, *145*, 65–73. [[CrossRef](#)]
26. Trueba, P.; Beltrán, A.M.; Bayo, J.M.; Rodríguez-Ortiz, J.A.; Larios, D.F.; Alonso, E.; Dunand, D.C.; Torres, Y. Porous Titanium Cylinders Obtained by the Freeze-Casting Technique: Influence of Process Parameters on Porosity and Mechanical Behavior. *Metals* **2020**, *10*, 188. [[CrossRef](#)]
27. Kim, S.W.; Jung, H.-D.; Kang, M.-H.; Kim, H.-E.; Koh, Y.-H.; Estrin, Y. Fabrication of porous titanium scaffold with controlled porous structure and net-shape using magnesium as spacer. *Mater. Sci. Eng. C* **2013**, *33*, 2808–2815. [[CrossRef](#)]
28. Jung, H.-D.; Yook, S.-W.; Jang, T.-S.; Li, Y.; Kim, H.-E.; Koh, Y.-H. Dynamic freeze casting for the production of porous titanium (Ti) scaffolds. *Mater. Sci. Eng. C* **2013**, *33*, 59–63. [[CrossRef](#)]
29. Lukaszewska-Kuska, M.; Wirstlein, P.; Majchrowski, R.; Dorocka-Bobkowska, B. Osteoblastic cell behaviour on modified titanium surfaces. *Micron* **2018**, *105*, 55–63. [[CrossRef](#)]
30. Li, T.; Gulati, K.; Wang, N.; Zhang, Z.; Ivanovski, S. Understanding and augmenting the stability of therapeutic nanotubes on anodized titanium implants. *Mater. Sci. Eng. C* **2018**, *88*, 182–195. [[CrossRef](#)]

31. Wang, Y.; Yu, H.; Chen, C.; Zhao, Z. Review of the biocompatibility of micro-arc oxidation coated titanium alloys. *Mater. Des.* **2015**, *85*, 640–652. [[CrossRef](#)]
32. Jang, T.-S.; Jung, H.-D.; Kim, S.; Moon, B.-S.; Baek, J.; Park, C.; Song, J.; Kim, H.-E. Multiscale porous titanium surfaces via a two-step etching process for improved mechanical and biological performance. *Biomed. Mater.* **2017**, *12*, 025008. [[CrossRef](#)]
33. Lee, H.; Jang, T.-S.; Song, J.; Kim, H.-E.; Jung, H.-D. Multi-scale porous Ti<sub>6</sub>Al<sub>4</sub>V scaffolds with enhanced strength and biocompatibility formed via dynamic freeze-casting coupled with micro-arc oxidation. *Mater. Lett.* **2016**, *185*, 21–24. [[CrossRef](#)]
34. Han, C.-M.; Kim, H.-E.; Koh, Y.-H. Creation of hierarchical micro/nano-porous TiO<sub>2</sub> surface layer onto Ti implants for improved biocompatibility. *Surf. Coat. Technol.* **2014**, *251*, 226–231. [[CrossRef](#)]
35. Civantos, A.; Giner, M.; Trueba, P.; Lascano, S.; Montoya-García, M.-J.; Arévalo, C.; Vázquez, M. Ángeles; Allain, J.P.; Torres, Y. In Vitro Bone Cell Behavior on Porous Titanium Samples: Influence of Porosity by Loose Sintering and Space Holder Techniques. *Metals* **2020**, *10*, 696. [[CrossRef](#)]
36. Jung, H.-D.; Yook, S.-W.; Han, C.-M.; Jang, T.-S.; Kim, H.-E.; Koh, Y.-H.; Estrin, Y. Highly aligned porous Ti scaffold coated with bone morphogenetic protein-loaded silica/chitosan hybrid for enhanced bone regeneration. *J. Biomed. Mater. Res. Part B Appl. Biomater.* **2013**, *102*, 913–921. [[CrossRef](#)] [[PubMed](#)]
37. Jung, H.-D.; Jang, T.-S.; Wang, L.; Kim, H.-E.; Koh, Y.-H.; Song, J. Novel strategy for mechanically tunable and bioactive metal implants. *Biofabrication* **2015**, *37*, 49–61. [[CrossRef](#)]
38. Kim, S.; Park, C.; Cheon, K.-H.; Jung, H.-D.; Song, J.; Kim, H.-E.; Jang, T.-S. Antibacterial and bioactive properties of stabilized silver on titanium with a nanostructured surface for dental applications. *Appl. Surf. Sci.* **2018**, *451*, 232–240. [[CrossRef](#)]
39. Heimann, R.B. Osseointegrative and Corrosion-Inhibiting Plasma-Sprayed Calcium Phosphate Coatings for Metallic Medical Implants. *Metals* **2017**, *7*, 468. [[CrossRef](#)]
40. Kim, H.; Choi, S.-H.; Ryu, J.-J.; Koh, S.-Y.; Park, J.-H.; Lee, I.-S. The biocompatibility of SLA-treated titanium implants. *Biomed. Mater.* **2008**, *3*, 025011. [[CrossRef](#)]
41. Ferguson, S.; Brogini, N.; Wieland, M.; De Wild, M.; Rupp, F.; Geis-Gerstorfer, J.; Cochran, D.; Buser, D. Biomechanical evaluation of the interfacial strength of a chemically modified sandblasted and acid-etched titanium surface. *J. Biomed. Mater. Res. Part A* **2006**, *78*, 291–297. [[CrossRef](#)] [[PubMed](#)]
42. Huang, C.-F.; Chiang, H.-J.; Lin, H.-J.; Hosseinkhani, H.; Ou, K.-L.; Peng, P.-W. Comparison of Cell Response and Surface Characteristics on Titanium Implant with SLA and SLA Affinity Functionalization. *J. Electrochem. Soc.* **2014**, *161*, G15–G20. [[CrossRef](#)]
43. He, W.; Yin, X.; Xie, L.; Liu, Z.; Li, J.; Zou, S.; Chen, J. Enhancing osseointegration of titanium implants through large-grit sandblasting combined with micro-arc oxidation surface modification. *J. Mater. Sci. Mater. Med.* **2019**, *30*, 73. [[CrossRef](#)] [[PubMed](#)]
44. Kim, S.; Park, C.; Moon, B.-S.; Kim, H.-E.; Jang, T.-S. Enhancement of osseointegration by direct coating of rhBMP-2 on target-ion induced plasma sputtering treated SLA surface for dental application. *J. Biomater. Appl.* **2016**, *31*, 807–818. [[CrossRef](#)]
45. Li, L.-H.; Kong, Y.-M.; Kim, H.-W.; Kim, Y.-W.; Kim, H.-E.; Heo, S.-J.; Koak, J.-Y. Improved biological performance of Ti implants due to surface modification by micro-arc oxidation. *Biofabrication* **2004**, *25*, 2867–2875. [[CrossRef](#)]
46. Tsutsumi, Y.; Niinomi, M.; Nakai, M.; Shimabukuro, M.; Ashida, M.; Chen, P.; Doi, H.; Hanawa, T. Electrochemical Surface Treatment of a  $\beta$ -titanium Alloy to Realize an Antibacterial Property and Bioactivity. *Metals* **2016**, *6*, 76. [[CrossRef](#)]
47. Wei, D.; Zhou, Y.; Wang, Y.; Jia, D. Characteristic of microarc oxidized coatings on titanium alloy formed in electrolytes containing chelate complex and nano-HA. *Appl. Surf. Sci.* **2007**, *253*, 5045–5050. [[CrossRef](#)]
48. Li, L.-H.; Kim, H.-W.; Lee, S.-H.; Kong, Y.-M.; Kim, H.-E. Biocompatibility of titanium implants modified by microarc oxidation and hydroxyapatite coating. *J. Biomed. Mater. Res. Part A* **2005**, *73*, 48–54. [[CrossRef](#)]
49. Wu, L.; Wen, C.; Zhang, G.; Liu, J.; Ma, K. Influence of anodizing time on morphology, structure and tribological properties of composite anodic films on titanium alloy. *Vacuum* **2017**, *140*, 176–184. [[CrossRef](#)]
50. Kuromoto, N.K.; Simão, R.A.; Soares, G.A. Titanium oxide films produced on commercially pure titanium by anodic oxidation with different voltages. *Mater. Charact.* **2007**, *58*, 114–121. [[CrossRef](#)]
51. Wang, H.-Y.; Zhu, R.-F.; Lu, Y.-P.; Xiao, G.-Y.; He, K.; Yuan, Y.; Ma, X.-N.; Li, Y. Effect of sandblasting intensity on microstructures and properties of pure titanium micro-arc oxidation coatings in an optimized composite technique. *Appl. Surf. Sci.* **2014**, *292*, 204–212. [[CrossRef](#)]
52. Zhan, X.; Li, S.; Cui, Y.; Tao, A.; Wang, C.; Li, H.; Linzhang, L.; Yu, H.; Jiang, J.; Li, C. Comparison of the osteoblastic activity of low elastic modulus Ti-24Nb-4Zr-8Sn alloy and pure titanium modified by physical and chemical methods. *Mater. Sci. Eng. C* **2020**, *113*, 111018. [[CrossRef](#)] [[PubMed](#)]
53. Graziano, A.; D’Aquino, R.; Angelis, M.G.C.-D.; De Francesco, F.; Giordano, A.; Laino, G.; Piattelli, A.; Traini, T.; De Rosa, A.; Papaccio, G. Scaffold’s surface geometry significantly affects human stem cell bone tissue engineering. *J. Cell. Physiol.* **2007**, *214*, 166–172. [[CrossRef](#)] [[PubMed](#)]
54. Kulkarni, M.; Patil-Sen, Y.; Junkar, I.; Kulkarni, C.V.; Lorenzetti, M.; Iglíč, A. Wettability studies of topologically distinct titanium surfaces. *Colloids Surf. B Biointerfaces* **2015**, *129*, 47–53. [[CrossRef](#)] [[PubMed](#)]
55. Hotchkiss, K.M.; Reddy, G.B.; Hyzy, S.L.; Schwartz, Z.; Boyan, B.D.; Olivares-Navarrete, R. Titanium surface characteristics, including topography and wettability, alter macrophage activation. *Acta Biomater.* **2016**, *31*, 425–434. [[CrossRef](#)]

56. Gittens, R.A.; Olivares-Navarrete, R.; Cheng, A.; Anderson, D.M.; McLachlan, T.; Stephan, I.; Geis-Gerstorfer, J.; Sandhage, K.H.; Fedorov, A.G.; Rupp, F.; et al. The roles of titanium surface micro/nanotopography and wettability on the differential response of human osteoblast lineage cells. *Acta Biomater.* **2013**, *9*, 6268–6277. [[CrossRef](#)]
57. Rosales-Leal, J.; Rodríguez-Valverde, M.; Mazzaglia, G.; Ramón-Torregrosa, P.; Díaz-Rodríguez, L.; García-Martínez, O.; Vallecillo-Capilla, M.; Ruiz, C.; Cabrerizo-Vílchez, M. Effect of roughness, wettability and morphology of engineered titanium surfaces on osteoblast-like cell adhesion. *Colloids Surf. A Physicochem. Eng. Asp.* **2010**, *365*, 222–229. [[CrossRef](#)]
58. Kim, S.-B.; Jo, J.-H.; Lee, S.-M.; Kim, H.-E.; Shin, K.-H.; Koh, Y.-H. Use of a poly(ether imide) coating to improve corrosion resistance and biocompatibility of magnesium (Mg) implant for orthopedic applications. *J. Biomed. Mater. Res. Part A* **2013**, *101*, 1708–1715. [[CrossRef](#)]
59. Cheon, K.-H.; Park, C.; Kang, M.-H.; Kang, I.-G.; Lee, M.-K.; Lee, H.; Kim, H.-E.; Jung, H.-D.; Jang, T.-S. Construction of tantalum/poly(ether imide) coatings on magnesium implants with both corrosion protection and osseointegration properties. *Bioact. Mater.* **2021**, *6*, 1189–1200. [[CrossRef](#)]
60. Kang, M.-H.; Jang, T.-S.; Jung, H.-D.; Kim, S.-M.; Kim, H.-E.; Koh, Y.-H.; Song, J. Poly(ether imide)-silica hybrid coatings for tunable corrosion behavior and improved biocompatibility of magnesium implants. *Biomed. Mater.* **2016**, *11*, 035003. [[CrossRef](#)]
61. İzmir, M.; Ercan, B. Anodization of titanium alloys for orthopedic applications. *Front. Chem. Sci. Eng.* **2019**, *13*, 28–45. [[CrossRef](#)]
62. Yu, W.Q.; Zhang, Y.L.; Jiang, X.Q.; Zhang, F.Q. In vitro behavior of MC3T3-E1 preosteoblast with different annealing temperature titania nanotubes. *Oral Dis.* **2010**, *16*, 624–630. [[CrossRef](#)] [[PubMed](#)]
63. Oh, S.; Daraio, C.; Chen, L.-H.; Pisanic, T.R.; Fiñones, R.R.; Jin, S. Significantly accelerated osteoblast cell growth on aligned TiO<sub>2</sub> nanotubes. *J. Biomed. Mater. Res. Part A* **2006**, *78*, 97–103. [[CrossRef](#)] [[PubMed](#)]
64. Brodie, J.C.; Goldie, E.; Connel, G.; Merry, J.; Grant, M.H. Osteoblast interactions with calcium phosphate ceramics modified by coating with type I collagen. *J. Biomed. Mater. Res. Part A* **2005**, *73*, 409–421. [[CrossRef](#)] [[PubMed](#)]